The physical simulation of a transient, downburst-like event – how complex does it need to be?

Jesson, Michael; Lombardo, F; Sterling, Mark; Baker, Christopher

DOI:
10.1016/j.jweia.2019.03.021

Document Version
Peer reviewed version

Citation for published version (Harvard):
Jesson, M, Lombardo, F, Sterling, M & Baker, C 2019, 'The physical simulation of a transient, downburst-like event – how complex does it need to be?', *Journal of Wind Engineering and Industrial Aerodynamics*, vol. 189, pp. 135-150. https://doi.org/10.1016/j.jweia.2019.03.021

The physical simulation of a transient, downburst-like event – how complex does it need to be?

Mike Jesson[1]*, Frank Lombardo[2], Mark Sterling[1] and Chris Baker[1]
[1]Department of Civil Engineering, University of Birmingham, Birmingham, UK.
[2]Department of Civil and Environmental Engineering, University of Illinois at Urbana-Champaign, Illinois, USA.
*m.a.jesson@bham.ac.uk

Abstract

There has been much debate of late regarding the physical simulation of downbursts and, in particular, the need to construct large-scale, relatively expensive facilities in order to obtain wind loading data. For the first time, this paper illustrates that, through the use of partial turbulence simulations and quasi-steady analysis, it is possible to capture the both the loading due to the large-scale features present in downburst flows and the local peaks due to smaller scales of turbulence. These findings have considerable implications for future analysis of transient winds.

1 Introduction

Thunderstorm downbursts are transient, non-synoptic wind events which form in storm convection cells. Although generally less well known than other non-synoptic events such as tornadoes, downbursts are the cause of the building design wind speeds in many parts of the world (Chay and Letchford, 2002a).

The rapid cooling of warm, moist air rising in a convection cell, expedited by evaporation of precipitation (Wakimoto and Bringi, 1988), creates a mass of cold, dense air. Thus the motion is reversed and a downdraft is formed, with a ring vortex forming around the edge of the downdraft region (see Vermeire et al (2011) for details). When the downdraft hits the ground a stagnation region forms, driving a radial outflow which carries this vortex (which has a height of ~0.7-1km (Hjelmfelt, 1988)) with it (Fujita, 1981). The combination of the outflow and the ring vortex leads to high wind speeds in the near ground region with, the maximum velocity occurring at a height z_m = 30-100m above the ground (Fujita and Wakimoto, 1981; Hjelmfelt, 1988). Further flow acceleration has been attributed to the formation of a counter-rotating secondary vortex at the leading edge of the primary (ring) vortex, as seen in numerical simulations (Kim and Hangan, 2007; Mason et al., 2009b). The downburst flow field experienced by a structure, or measured by a fixed anemometer, is further complicated by the translation of the entire downburst as it moves within the parent storm. This translation results in large changes of wind direction as the impingement point moves relative the structure itself, and direction changes are also seen around the time of peak velocity (Lombardo et al., 2018) though these changes take place over timescales of the order of tens of seconds or greater.

Microbursts, as Fujita (1981) terms the most intense downbursts, are relatively small in both temporal and spatial scale, with a downdraft diameter of approximately 1km and a period of extreme wind speed lasting approximately 5 minutes (Fujita, 1981; Holmes et al., 2008). This presents difficulties in recording full-scale events or making full-scale measurements of wind loading on structures during a downburst. Historic projects such as NIMROD and JAWS (Fujita, 1981), and the more recent Thunderstorm Outflow Experiment (Gast and Schroeder, 2003; Holmes et al., 2008)

have succeeded in recording a small number of full-scale downbursts. When considering wind loading on structures, the unpredictability of where and when a downburst will strike makes it very difficult to obtain full-scale pressure measurements over a structure – the chances of a single, instrumented building being subject to a downburst are extremely small. Lombardo (2009) has, however, successfully identified a small number of downburst events from historical velocity data recorded at the Texas Tech University Wind Engineering Field Research Laboratory (WERFL), and examined the corresponding pressure data from tappings over the WERFL building (a 9m x 14m x 4m tall, rectangular plan building) – with one case recently detailed in Lombardo et al. (2018)..

Although Lombardo et al. have successfully measured downburst wind loading at full-scale, their data is limited to a single type of building and is unavoidably restricted in the range of parameters by the events which have occurred at the field site. Therefore, as with Atmospheric Boundary Layer (ABL) studies, physical simulation is required to determine downburst wind loading on different types and style of structure. A number of physical simulation methods have been applied in order to model downbursts at laboratory-scale: very small-scale density driven flows (e.g. Lundgren et al., 1992); multi-fan wind tunnels (e.g. Butler et al., 2010); slot jets (e.g. Butler and Kareem, 2007; Lin et al., 2007); steady and pulsed impinging jets (e.g. Chay and Letchford, 2002a, 2002b; Choi, 2004; Wood et al., 2001; Zhang et al., 2014, 2013 and Haines et al., 2013; Jesson et al., 2015b, 2015a; Mason et al., 2009a; McConville et al., 2009 respectively). The development of the pulsed jet and slot jet simulators has been driven by the assumption that it is necessary to simulate the transient nature and vortices of a full-scale downburst. The latter has been considered a requirement due to the approximately building-scale primary and secondary vortices which are a feature of many downbursts, with the implicit assumption that the vertical component is non-negligible and must be simulated. Surprisingly, despite the efforts made to generate these vortices and their vertical velocity, these studies have tended to focus solely on the radial (horizontal) velocity component for validation of the wind field.

The development of these simulators has permitted wind loading on a variety of model-scale structures to be measured. Direct measurements of loading on pressure tapped building models have been made (e.g. Chay and Letchford, 2002b, 2002a; Jesson et al., 2015b, 2015a; Mason et al., 2009a). Additionally, the physical simulation data has been used to validate CFD simulations which have then been applied to calculate loading on, and failure of, power transmission lines exposed to downbursts (e.g. Aboshosha and El Damatty, 2015; Shehata et al., 2005). Although such projects provide valuable loading data, the number of types of structures for which data is currently available is limited. The complexity of the simulators makes them expensive and the experimental process slow, while the small scale (1:1600 in the work of Jesson et al., for example) limits the measurements which can be made, the size and detailing of the models and precision of probe placement. As a consequence, current design codes either have no provision for downburst loading, or simply apply a factor to ABL loading pressure coefficients.

This paper determines whether such complex physical simulations are required for downburst wind loading studies. Data from full-scale downburst events is analysed, focussing on the length scales of the large- and small-scale structures of the wind field and the vertical velocity component at building height. This introduction is followed by a discussion of pertinent theory (Section 2), the methodology applied (Section 3), and in Section 4 by a presentation and discussion of the results. The paper concludes with a summary of the important implications of this work.

2 Background

2.1 Non-Stationary Analysis

In the case of statistically stationary winds, the turbulence intensity of a velocity component, I_x (where $x = u,v,w$, and u, v and w are the instantaneous, raw streamwise, lateral and vertical velocity components respectively), is generally defined as the ratio of the standard deviation of the component, σ_x, to the mean streamwise velocity, U (Holmes, 2001):

$$I_x = \frac{\sigma_x}{U} \tag{1}$$

Downburst wind fields are statistically highly non-stationary, and as a consequence, this definition is problematic as neither σ_x nor U are clearly defined in the case of a non-stationary time-series. While there is currently no standard method for doing so, a time-varying streamwise turbulence intensity may be calculated by decomposing the streamwise velocity time-series into a time-varying mean, $U(t)$, and a residual fluctuating component, $u'(t) = u(t) - U(t)$ (similarly for v' and w'). This decomposition has previously been achieved through two methods. The first is through defining $U(t)$ as a simple, N-point moving average (Holmes et al., 2008). In previous studies N has been taken as a value which is judged "reasonable" based on the resulting $U(t)$ and $u'(t)$ time-series capturing the main flow features and having a near-zero mean respectively (Holmes et al., 2008). However, the effective cut-off frequency, f_c, of a moving average filter applied to a time-series sampled at rate f_s, with averaging over a period $\Delta t = f_s N$ may be estimated as (Asghari Mooneghi et al., 2016):

$$f_c \cong \frac{0.45}{\Delta t} \tag{2}$$

if $f_s \gg f_c$.

The second method is wavelet decomposition (Jesson et al., 2015b; Wang, 2007; Wang and Kareem, 2004; a similar approach has been applied by Chen and Letchford, 2005). Wavelet analysis uses the convolution of scaled and translated versions of a parent wavelet to determine the time-varying power spectral density of a time-series. The parent wavelet can have a variety of forms, but must be defined by a zero-mean function which is localised in time and frequency (Torrence and Compo, 1998).

The Continuous Wavelet Transform (CWT) algorithm (Torrence and Compo, 1998) outputs a 2-D matrix of wavelet coefficients, each corresponding to a wavelet scale and time. The scales may be converted to a pseudo-frequencies through multiplication by an appropriate velocity scalar. In what follows, the pseudo-frequency is referred to simply as frequency for convenience. In order to decompose the time-series, those coefficients corresponding to frequencies above (or below) the required cut-off frequency are set to zero and the inverse CWT algorithm (Erickson, 2016) applied to give the low-frequency (or high-frequency) component.

Once the signal has been decomposed into $U(t)$ and $u'(t)$ the time-varying $I_u(t)$ is calculated as:

$$I_u(t) = \frac{\overline{\sigma_{u',T}}(t)}{\overline{U_T}(t)} \tag{3}$$

where overbar and subscript T indicate the time-mean over an interval of T seconds around time t (Holmes et al., 2008; Wang et al., 2013).

In application to downburst flows, a second issue with the definition of turbulence intensity in (1) arises. Implicit in (1) (and consequently (3)) is the assumption that mean velocities in the lateral and vertical directions are negligible, i.e. that the mean flow speed may be approximated as U, and the flow has a clearly defined streamwise direction. This will not be the case for a downburst flow field, which is frequently modelled as a combination of large-scale vortices (e.g. Fujita, 1985; Mason et al., 2009b). In order to account for these additional non-negligible components, (3) has been amended to:

$$I_x(t) = \frac{\overline{\sigma_{x',T}}(t)}{\overline{S_T}(t)} \tag{4}$$

where $S(t)$ is the instantaneous wind speed:

$$S(t) = \sqrt{u^2(t) + v^2(t) + w^2(t)} \tag{5}$$

Clearly this change will have negligible effect if $v(t)$ and $w(t)$ are approximately zero-mean.

2.2 Quasi-Steady Theory

Quasi-steady (QS) theory assumes that the pressure at a point on the building envelope is proportional to a dynamic pressure, $\frac{1}{2}\rho U_{ref}^2$, calculated from a reference wind speed, U_{ref}, and the air density, ρ (Letchford et al., 1993). The constant of proportionality is the pressure coefficient, C_p, with the differential pressure, Δp (pressure relative to a reference pressure), given by:

$$\Delta p = C_p \frac{1}{2}\rho U_{ref}^2 \tag{6}$$

For ABL flow, time variation of the pressure field due to turbulence is incorporated through the use of instantaneous wind speed, $U_{ref}(t)$:

$$\Delta p(t) = \frac{1}{2}\rho C_p U_{ref}^2(t) \tag{7}$$

C_p varies over the building envelope (Figure 1) thereby accounting for, for example, regions of flow separation (in which $C_p < 0$) on the roof and leeward face, and high pressure regions on windward faces (where $C_p > 0$). It is clear that as the angle of the incoming wind (the azimuth, θ) varies then these regions change location on the building. Consequently C_p at a particular point is a function of θ and, similarly, C_p is dependent on the angle of the wind to the horizontal, the elevation, β. Hence $C_p = C_p(\theta,\beta)$ (Wu and Kopp, 2018, 2016) and is inherently time-varying since u, v and w vary with time:

$$\theta = \tan^{-1}\left(\frac{v(t)}{u(t)}\right) \tag{8}$$

$$\beta = \tan^{-1}\left(\frac{w(t)}{\sqrt{u^2(t) + v^2(t)}}\right) \tag{9}$$

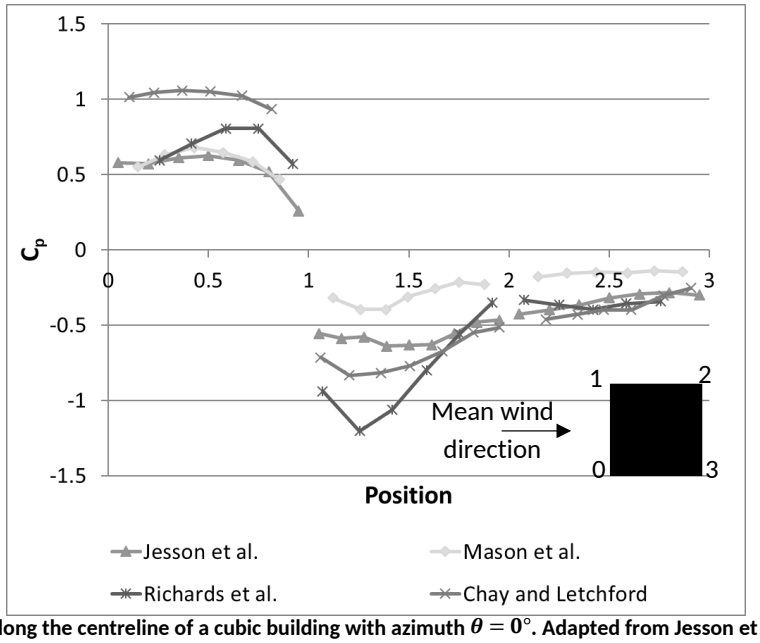

Figure 1 C_p along the centreline of a cubic building with azimuth $\theta = 0°$. Adapted from Jesson et al. (2015b). Original data from downburst simulations (Jesson et al. (2015b), Mason et al. (2009a), Chay and Letchford (2002a)) and full-scale ABL flow (Richards et al. (2001)).

For practical application, i.e. calculation of wind loading under expected wind fields, C_p must be quantified for the type of building and the expected range of θ and β. This is generally achieved through physical simulations in which Δp and U_{ref} are measured simultaneously and θ and β are varied by rotation and tilting of the building model (e.g. Letchford and Marwood, 1997; Richards and Hoxey, 2004). From such tests it has been found that if v and w are assumed to be small relative to u then the variation in C_p with angle may be represented by a simple, linear expansion (Letchford et al., 1993):

$$C_p(\theta, \beta) = C_p(\overline{\theta},\overline{\beta}) + \left(\frac{v}{U}\right)\frac{dC_p}{d\theta} + \left(\frac{w}{U}\right)\frac{dC_p}{d\beta} \tag{10}$$

where overbars (angles) and capitals (velocities) indicate time-mean values. Conversely, Richards et al. (1995) show that for larger v (w was not considered) the pressure coefficient data for a tapping at the leading roof edge of a building is periodic in θ and so a fitted Fourier series gives a good approximation:

$$C_p(\theta) = \sum_{k=0}^{N} a_k \cos(k\theta) + b_k \sin(k\theta) \tag{11}$$

where a_k and b_k are the fitted Fourier coefficients. As any such function $C_p(\theta)$ is necessarily periodic over the range $-\pi \leq \theta < \pi$, it should be possible to determine an equivalent Fourier series for any tapping position.

In the discussion which follows it is assumed that experiments may be designed to measure C_p for all required combinations of θ and β.

2.3 Partial Turbulence Simulation

Richards and Hoxey (2004) note "*that a quasi-steady model cannot be expected to account for every effect*", and it is recognised that peak wind pressures are influenced by both large-scale turbulence (accounted for by quasi-steady theory) and small-scale turbulence in the incoming wind field which interacts with building generated turbulence and shear layers (Asghari Mooneghi et al., 2016); the effects of the latter cannot be modelled by quasi-steady theory, a limitation which is accepted for ABL simulations. Asghari Mooneghi et al. (2016) considered the relevance of these two scales of turbulence in wind tunnel modelling of a low-rise building. In contrast to the modelling of high-rise buildings, which typically requires model scales smaller than 1:300, modelling low-rise buildings at a practical size requires large model scales. At these larger model scales, the large-scale turbulence of ABL flow cannot be simulated within a standard wind tunnel (Asghari Mooneghi et al., 2016; Wu and Kopp, 2018). This limitation can be mitigated through "Partial Turbulence Simulation" (PTS), in which the contribution of small-scale turbulence is quantified through wind tunnel experiments in which these small-scales are correctly simulated, with a quasi-steady approach used to account for the large-scale turbulence in post processing (Asghari Mooneghi et al., 2016). Comparison with full-scale data showed that peak pressure coefficients "*agreed well enough*" (Asghari Mooneghi et al., 2016), with the largest errors being around 20% and generally much lower. Asghari Mooneghi et al. make an assumption which is problematic when directly applying their method to a transient event - the streamwise high frequency turbulence intensity, I_{uH}:

$$I_{uH} = \frac{\sigma_{uH}}{U + u_L} \tag{12}$$

is assumed constant (subscripts L and H signify low and high frequency components, i.e. small- and large-scale turbulence, respectively). As has been shown (e.g. Holmes et al., 2007; Jesson et al., 2015b) this is not the case for downbursts. However, the main application of this assumption is in the determination of the boundary frequency between large- and small-scales, which includes the somewhat arbitrary ratio of 1:10 for the building height to the cut-off length scale. Wu and Kopp (2018) further investigated the PTS approach in a set of wind tunnel tests investigating upstream roughness/turbulence effects, again focussing on the roof of a low-rise building, with $13\% \leq I_u \leq 27\%$ and azimuths $0° \leq \theta \leq 90°$. Elevation variation was purely due to turbulence in the flow (i.e. their models were not tilted). Building surface pressures were measured simultaneously with wind velocity at one roof height above the leading edge of their building model. Through examination of the coherence between quasi-steady predictions and measured pressure coefficient, Wu and Kopp determined that $5H$, where H is the building height, was an appropriate cut-off scale for low-rise buildings.

Both Asghari Mooneghi et al. (2016) and Wu and Kopp (2018) define the boundary frequency between small and large-scale turbulence in terms of the building height. It should be noted that (as stated by the former) the matching of this frequency at model and full-scale is based on some representative length rather than the height specifically, with the height considered appropriate for low-rise buildings.

3 Methodology

In the current paper, the requirement for transient physical simulations of downburst wind fields is assessed by examination of two factors:

1) The extent to which the transient flow field can be modelled using a quasi-steady approach, with small-scale turbulence being a zero-mean time-series, the effects of which can be accounted for in a similar manner to the PTS approach.
2) The importance of the vertical component of velocity (as discussed later, the lateral component is assumed negligible), which is predicted to exist due to the ring and secondary vortices of a "standard" downburst.

The data analysed are full-scale, horizontal and vertical wind speed data recorded at the Texas Tech University Wind Engineering Research Field Laboratory (WERFL) field site during five transient wind events identified as downbursts. Details of the site and transient wind detection are given by Lombardo et al. (2014). Briefly, the original WERFL, which was equipped with a 50m anemometer tower, was moved to a new site with a 200m tower in early 2006. The data were recorded by a network of anemometers at WERFL, with anemometers at height above ground, z, ranging from 1m to 200m. Data are not available for all events at all heights; details are given in Table 1. All anemometers were sampled at 30Hz. Both sites are classified as "open terrain" with z_0 approximately 0.015m. Additionally, a single stationary record of ABL flow from the same site has been processed in the same manner as a baseline.

Table 1 Anemometer heights for the recorded full-scale events

Date → / z (m) ↓	Stationary	19 June 2003	21 May 2008	19 June 2008	13 August 2008	08 March 2010
200	x		x	x	x	x
158	x		x	x	x	x
75	x					x
49		x				
47	x					x
21		x				
17	x					x
10	x	x	x	x	x	x
4	x	x	x	x	x	x
2		x	x	x	x	
1			x	x	x	

The anemometers record horizontal and vertical wind speeds, rather than 3-D velocities. Henceforth it is assumed that, as the downburst flow is driven by a localised impingement point which results in high-speed radial winds, the flow may be treated as a 2-D flow with only streamwise and vertical components and negligible lateral velocity, i.e. $v(t) \equiv 0$. It should be noted, however, that the streamwise direction is not fixed and may vary over timescales of minutes due to storm translation, as discussed in Section 1.

Wavelet decomposition (depicted in a flow chart in the Appendix for clarity) has been performed using the Morlet wavelet, $\psi_0(\eta)$, where η is a dimensionless "time". This is a modulated sinusoid defined as (Torrence and Compo, 1998):

$$\psi_0(\eta) = \pi^{-\frac{1}{4}} e^{i\omega_0\eta} e^{-\frac{\eta^2}{2}} \quad (13)$$

and was chosen due to its relationship to the sinusoids of the Fourier transform for a stationary time-series. ω_0 is the non-dimensional frequency. The cut-off frequency was based on the $5H$ limit of Wu and Kopp (2018), with a building heights of $H = 6m$ giving a cut-off scale of $30m$. Data up to a height of $z = 200m$ has been analysed, well above the height of a low-rise building. These data are put into context in the discussion of application in Section 5.2. An additional building height of $30m$ (corresponding to the upper end of the "low-rise" limit specified for downbursts by Jesson et al. (2015a)) has also been applied in a small number of cases to demonstrate its impact. Differences between this limit and the $10H$ limit of Asghari Mooneghi et al. (2016) were examined but found to be negligible (as demonstrated in Section 4). The Fourier periods returned by the CWT algorithm were converted to length scales through scaling by a representative streamwise wind speed, u_R:

$$u_R = u_{min30} + \frac{1}{2}(u_{max30} - u_{min30}) \quad (14)$$

where u_{max30} and u_{min30} are the maximum and minimum of $u_{30}(t)$ ($u(t)$ smoothed with a 30 second moving average. This moving average period was deemed to adequately smooth extremes. It is accepted that a different period, and indeed a different definition of u_R, may be applied. The aim of this process is, however, simply to obtain a representative speed for the conversion of the Fourier periods to approximate length scales, and so this method is considered appropriate). The first length scale exceeding $5H$ was identified, and taken to be the cut-off scale, corresponding to the cut-off frequency.

It is noted that the applicability of this $5H$ limit has not been proven for buildings as tall as $30m$, but it seems reasonable to assume that, if anything, the factor of 5 would be reduced in this case as the ratio of height to breadth and length increases. Consequently, retaining this relationship represents an extreme case in which medium-scale turbulence is included as "small" rather than "large". From this decomposition, the time-varying turbulence intensity and the form of the residual (high frequency) velocity are examined.

For comparison, decomposition has also been performed using a moving average decomposition. In this case, the moving average period was determined via (2) by setting f_c as used for the wavelet decomposition.

u_R was also used to define the period of highest wind speeds ("peak period"), taken as the period around the time of the maximum of $u_{30}(t)$ for which $u_{30}(t) \geq u_R$.

Integral length scales have been calculated as the integral of the autocorrelation function, $A_x(\tau)$ ($x = u,w$; τ is the time offset) for the range $0 \leq \tau \leq \tau_0$ (τ_0 is the first value for which $A_x(\tau) \leq 0$), scaled by u_R:

$$A_x(\tau) = \frac{1}{\sigma_x^2} \int_{t=0}^{t=T} x(t)x(t-\tau)dt \quad (15)$$

$$L_x = u_R \int_{\tau=0}^{\tau=\tau_0} A_x(\tau) d\tau \tag{16}$$

To investigate the vertical component of velocity, (9) was applied to the low-frequency time-series (similar results are obtained from the unfiltered time-series) to calculate the elevation angle time-series, $\beta(t)$. The wind speed measurements, $S(t)$, were split into bins based on the corresponding $\beta(t)$, with 5 degree bin widths, and the maximum wind speed from each bin identified to produce an elevation-based, maximum speed wind rose, used in Section 4.2.2. The duration of periods of "High-Speed, Large-Elevation" (HSLE) velocities were determined through cross-referencing the wind speed and elevation angle time-series. Continuous periods during which the wind had both a speed and elevation angle from the horizontal exceeding threshold values were identified, and the duration of each such section (the "HSLE Duration") calculated. A parametric study of the HSLE Duration was carried out, with a small range of speed and elevation thresholds. Due to the variability of the maximum wind speed, S_{max}, from event to event, the speed thresholds were set relative to this maximum, at $S_{max}/4$, $S_{max}/3$ and $S_{max}/2$. These factors were chosen as the smallest of these, $S_{max}/4$, would represent a wind speed of approximately $17ms^{-1}$ (approaching gale force) for an extreme microburst such as that recorded at Andrews Air Force Base (Fujita, 1985), and the others are convenient scalings. Elevation thresholds of $30°$ and $45°$ were used, based on an initial analysis of the elevation angles which occurred.

4 Results and Analysis

4.1 Stationary Data

The stationary data (Figure 2) follow the standard log-law profile, with increasing mean speed with height (Figure 3). Turbulence intensity, I_u, is relatively low (17% at $z = 4m$) but consistent with the site terrain ($z_0 \cong 0.015$ (Lombardo et al., 2014)) and the corresponding ESDU profiles (ESDU, 2001), and decreases with altitude as expected (Figure 3).

The time-varying I_u also decreases with height (not shown) and is generally below the stationary I_u value (Figure 4). This is consistent with the decomposition approach, in which the larger scales of turbulence are incorporated in the time-varying mean. By definition, the time-varying I_u depends on the building height due to the $5H$ scale boundary. As building height increases the cut-off scale is increased, resulting in more Fourier Periods included in $u'(t)$ and a larger $\sigma_{u'}$, and vice-versa. The time-varying I_u is therefore increased for $H = 30m$ (Figure 4(b)). The wavelet decomposition and moving average decomposition follow the same trends, with differences at extreme values (Figure 5). It is clear that, unlike the stationary I_u (which is seen as an absolute characteristic of the wind field), the time-varying $I_u$must be treated with caution, particularly when making comparisons across applications.

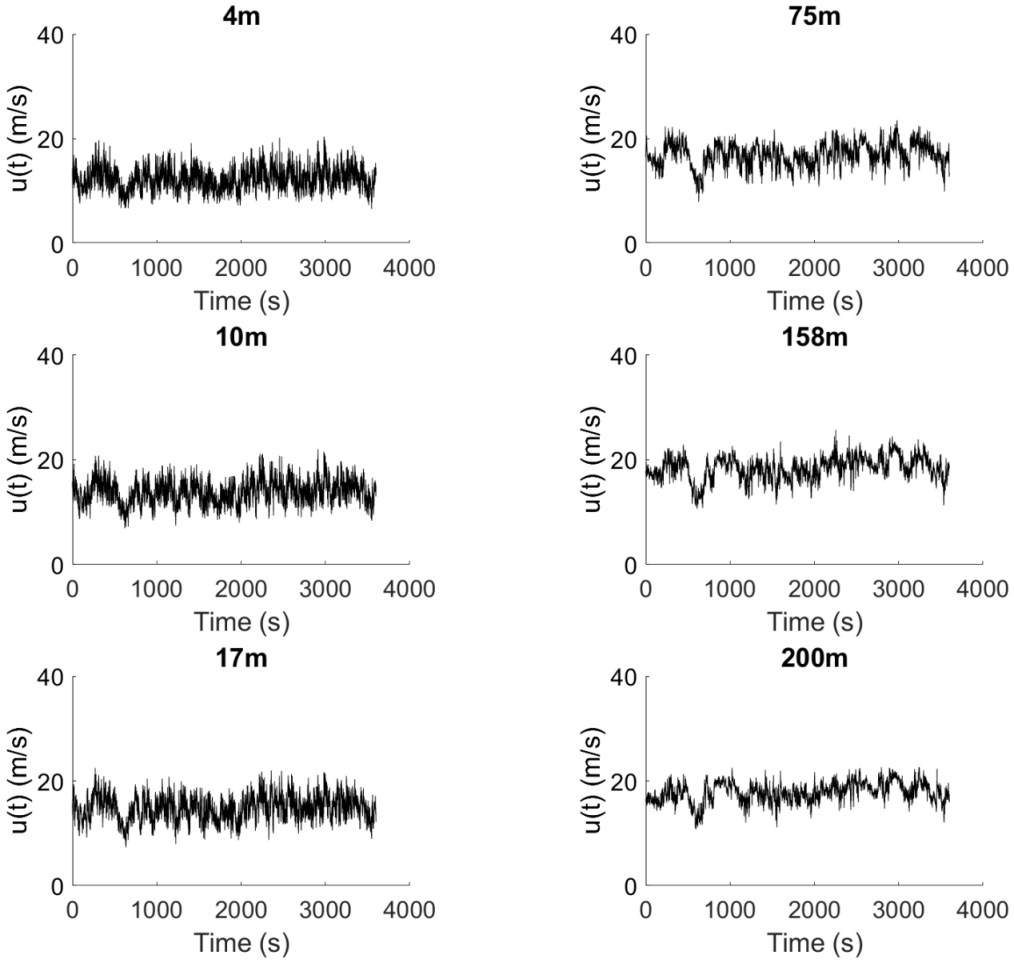

Figure 2 Streamwise velocity data for ABL flow at the test site

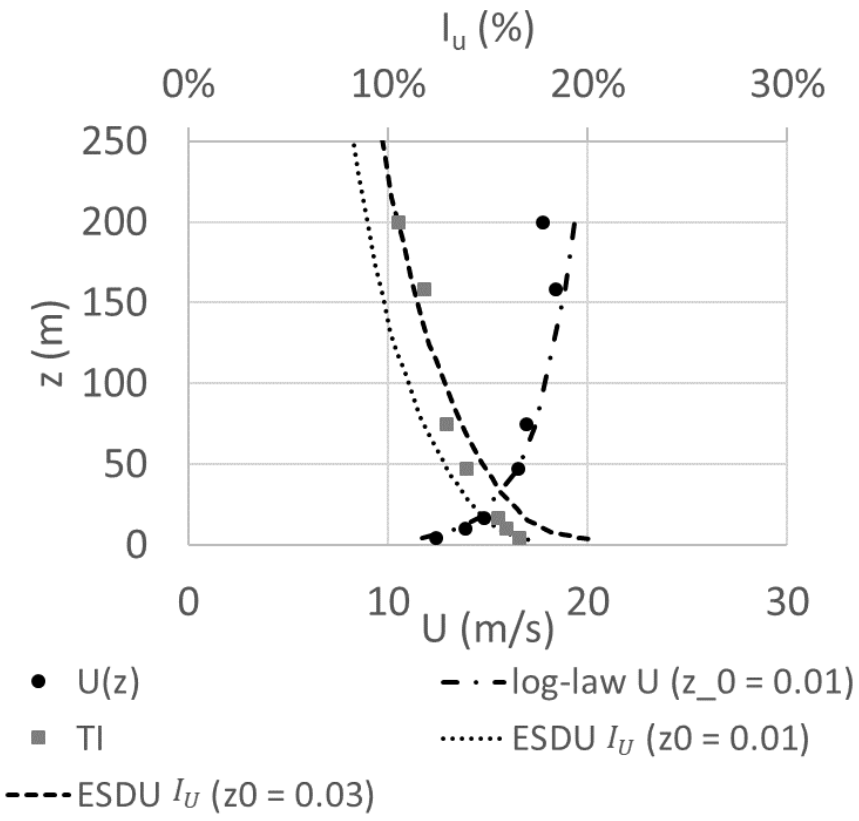

Figure 3 Mean wind speed and turbulence intensities for the stationary data

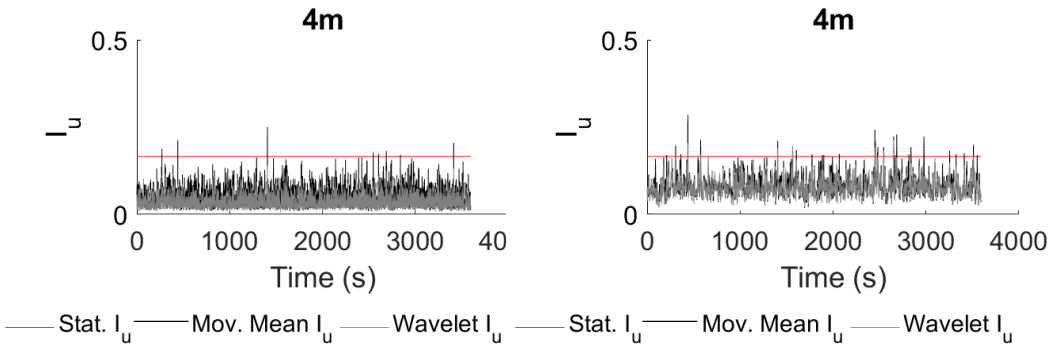

Figure 4 Turbulence Intensity of the stationary signal at $z = 4m$ with (a) $H = 6m$ and (b) $H = 30m$

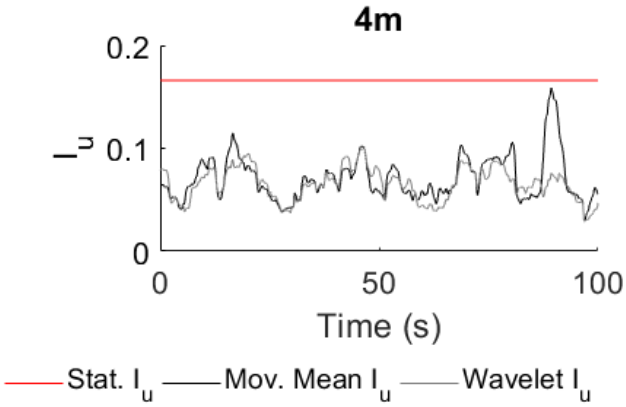

Figure 5 Sub-section of the turbulence Intensity of the stationary signal at $z = 4m$ with $H = 30m$

The effect of this change of cut-off frequency is also apparent in the high- and low-frequency decomposition (Figure 6). For the higher building ($H = 30m$) the low-frequency wind speed, $U(t)$, is smoothed in comparison with the low-rise case ($H = 6m$), while the root-mean-square (RMS) high-frequency wind speed, $u'(t)$, increases.

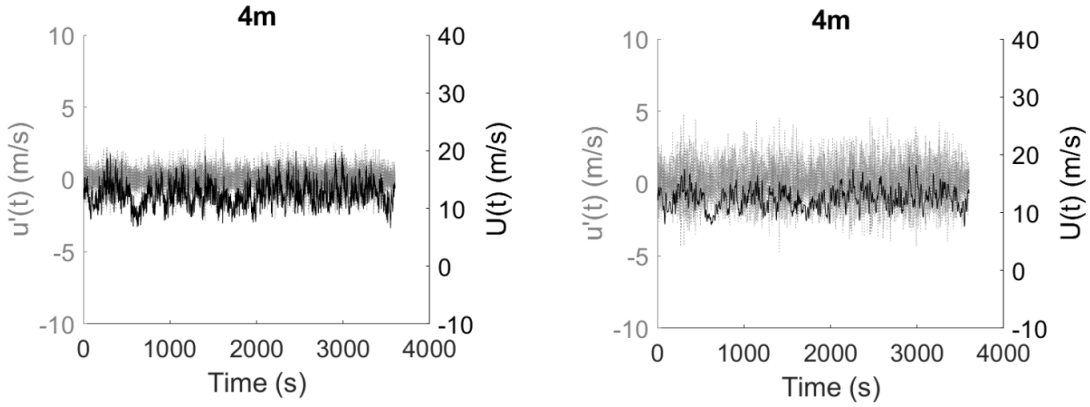

Figure 6 Wavelet decomposition of the stationary signal with (left) $H = 6m$ and (right) $H = 30m$.

4.2 Transient Events

4.2.1 Horizontal Wind Speed

It is recognised that there is a large variation in the velocity field between different downburst events (e.g. Choi, 2004; Hjelmfelt, 1988; Lombardo, 2009; Zhang et al., 2018). This is further evidenced by the events recorded for the current study (Figure 7). Four events show a clear acceleration in the horizontal wind speed, though the rate of acceleration and duration of the high wind speeds differ from event to event. For each event, the horizontal wind speed time-series are qualitatively the same across all measured heights (Figure 8).

With the exception of a small number of cases, the data of 13th August 2008 event are representative of all downburst events analysed. Data from this event are presented as representative of all events, with data from other events included only where important differences occur, or similarities are to be clearly demonstrated.

Wavelet decomposition, with the cut-off frequency/scale determined by the $5H$ relationship, splits the wind speed time-series into a slowly fluctuating component, which follows the large-scale features of the flow field, and a rapidly fluctuating component (Figure 9). Importantly, although the magnitude of the latter varies with time, this variation is slow in relation to the frequencies making up the component, i.e. it is effectively a modulation of a stationary signal. (This representation of the stochastic part of the flow has been applied in numerical simulations of downbursts, e.g. Chen and Letchford, 2007; Kwon and Kareem, 2009; Solari, 2016). It is not unreasonable to conclude, therefore, that the peak wind loading due to this high-frequency part of the downburst wind field (for which, under the PTS assumption, the quasi-steady approach is not suitable), can be quantified experimentally using steady, suitably turbulent flow and the same statistical methods previously applied for ABL flow.

There is a general trend of an increase in the magnitude of the residual, high-frequency component as the low-frequency component increases (Figure 9). This is particularly evident for those events with a low initial wind speed and clear increase during the downburst itself. The magnitude of the high-frequency component reduces with altitude (Figure 10), and this manifests itself as a reduction in time-varying turbulence intensity (Figure 11), as seen for ABL flows. Following Holmes et al. (2008), the mean turbulence intensity during the peak period (defined in Section 2) has been calculated. From Figure 11 it is evident that there are issues with this calculation. Firstly, the peak period is not necessarily the same across heights. Refinement of the definition may aid with this, but in the example shown the wind speed exhibits a double peak at low altitudes, while at higher altitudes these peaks are merged (though this is specific to this particular event, which has a longer peak duration than others). Secondly, the turbulence intensity is not constant across the peak period, and this variation is not consistent across events or altitude, beyond a tendency to increase at the start and end of the peak period, attributable to the lower $S(t)$ at these times. The reduction with height of the turbulence intensity during the peak period is evident, falling from between 13% and 18% at $z = 1m$ to 1% at $z = 200m$ (Figure 12). The rapid reduction in I_u with height may be due to the relatively short development length (and thus thinness) of the local boundary layer which develops with the downburst outflow. Integral length scales of turbulence for the high-frequency component reduce with building height (Figure 13), consistent with the reduction in the cut-off scale. Some spread is seen from event-to-event, particularly at low altitudes. At $z \geq 10m$, L_u is

consistent with the stationary case, indicating that if an ABL tunnel is able to adequately simulate the required scales for ABL flow then it can also do so for a downburst-like flow. The maximum integral length scales seen are approximately $10m$, two orders of magnitude smaller than both the downdraft diameter ($\sim 1000m$) or the ring vortex diameter (estimated as $700m$ to $1100m$ (Hjelmfelt, 1988)). The issue of how to correctly determine the scaling of downburst simulations is an open one, with one of these two parameters commonly used as a length scale, though with limited justification. Replacing pulsed/impinging jet simulations with a quasi-steady/PTS approach removes the requirement for such simulations and renders these scaling arguments redundant.

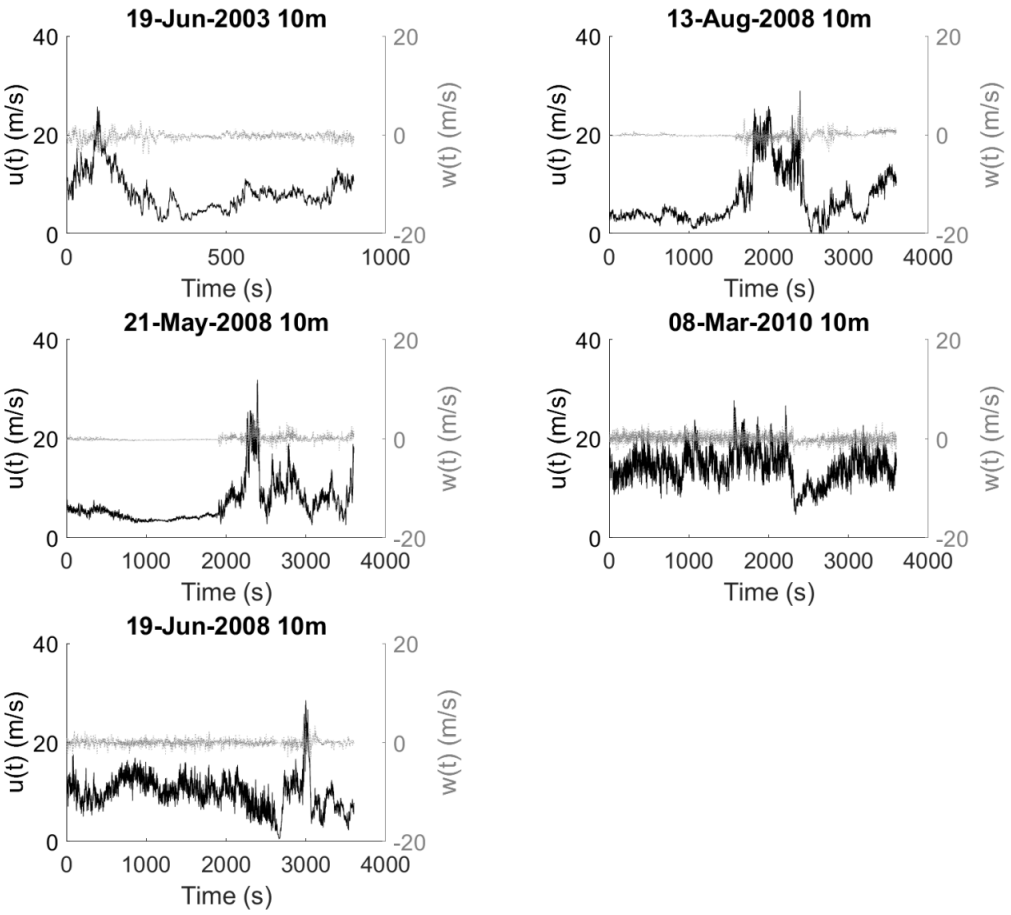

Figure 7 Velocity time-series at 10m for five downburst events.
$t = 0$ is the start of the 1 hour period during which the event was detected.

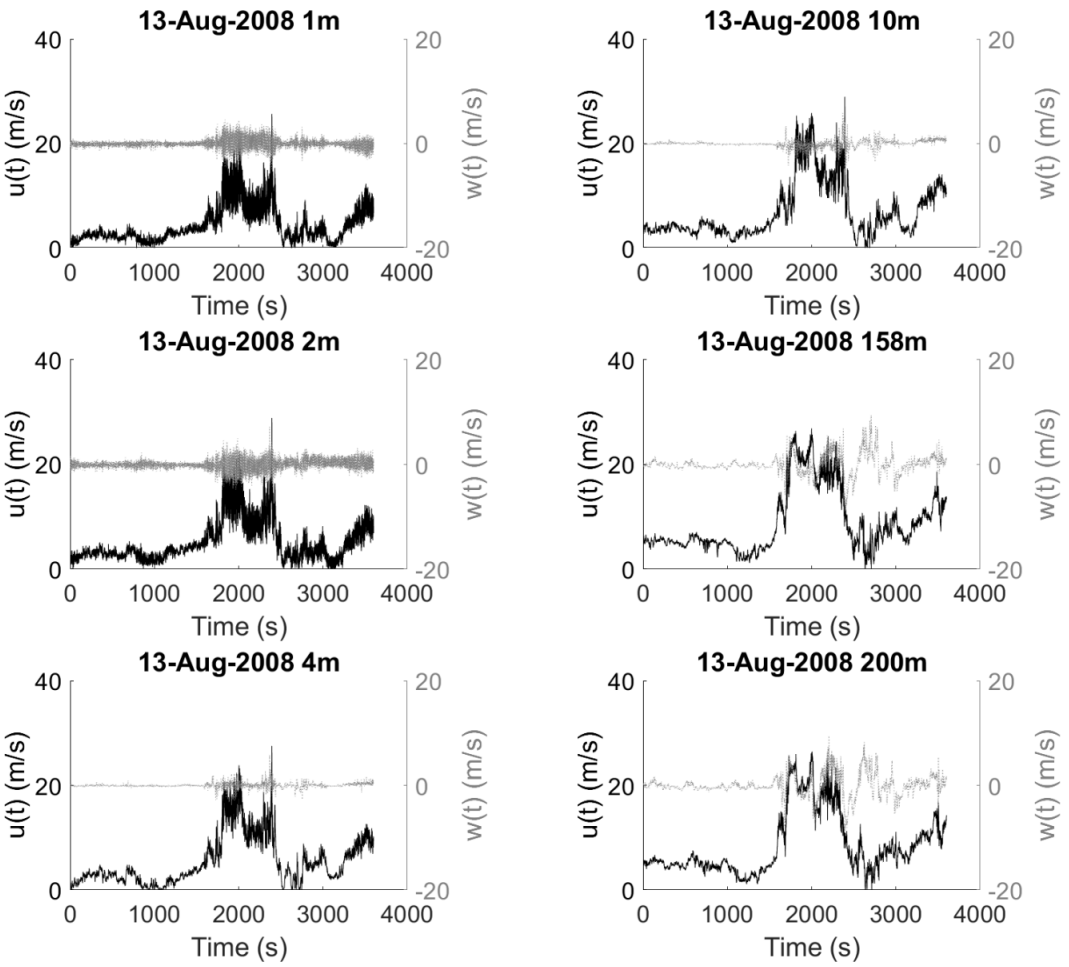

Figure 8 Velocity time-series for the 13th August 2008 event at a different heights above the ground

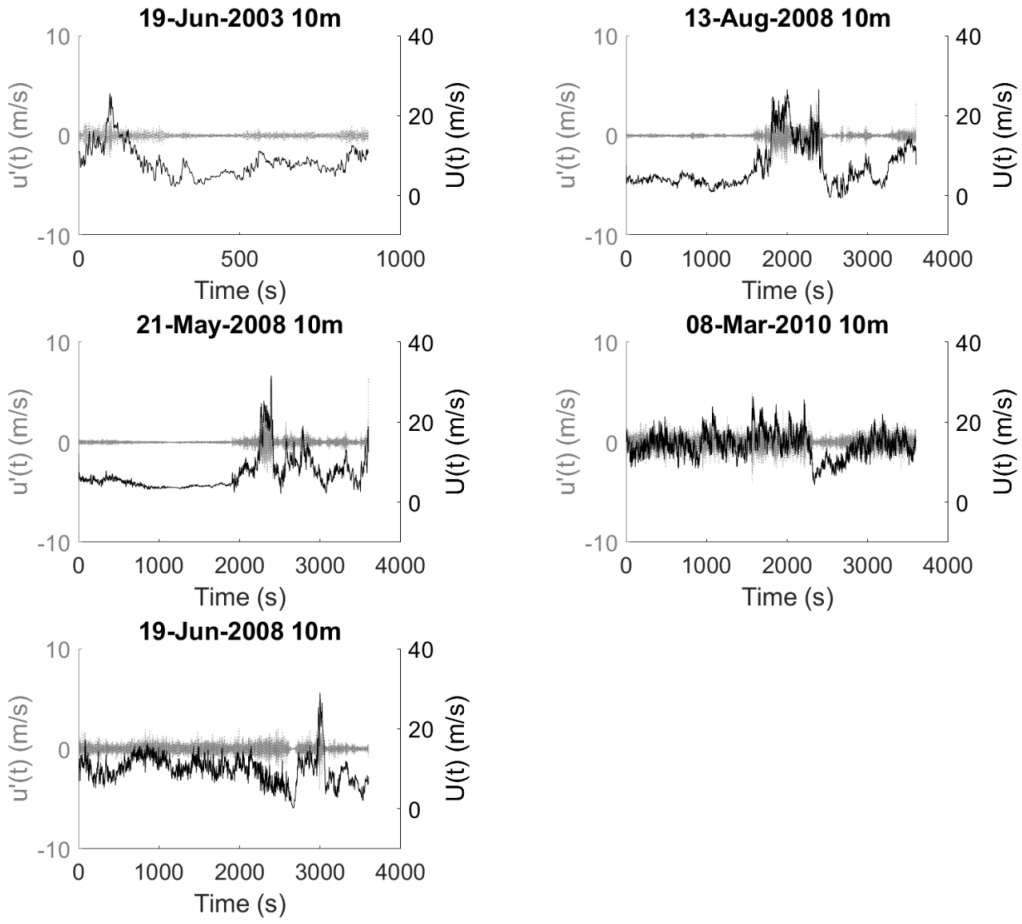

Figure 9 Wavelet decomposition of the horizontal wind speed at 10m for five downburst events

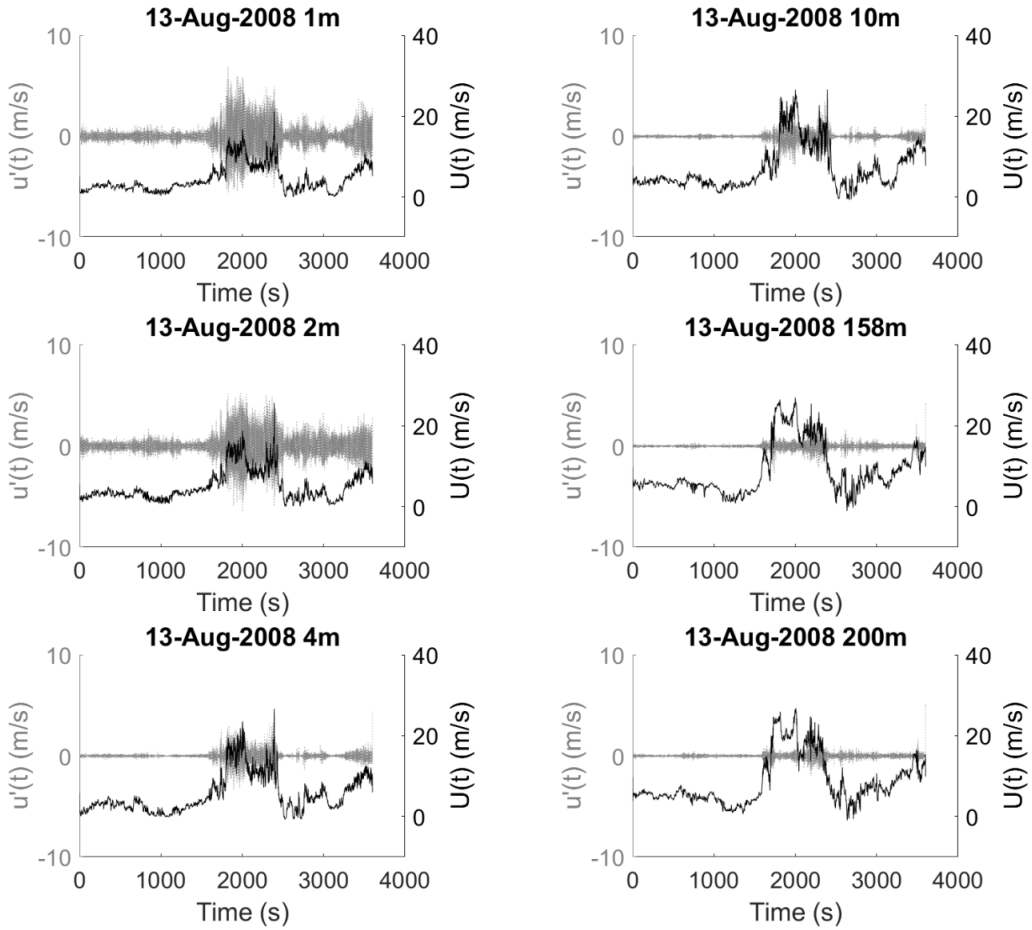

Figure 10 Wavelet decomposition of the horizontal wind speed for the 13th August 2008 event at all measured heights

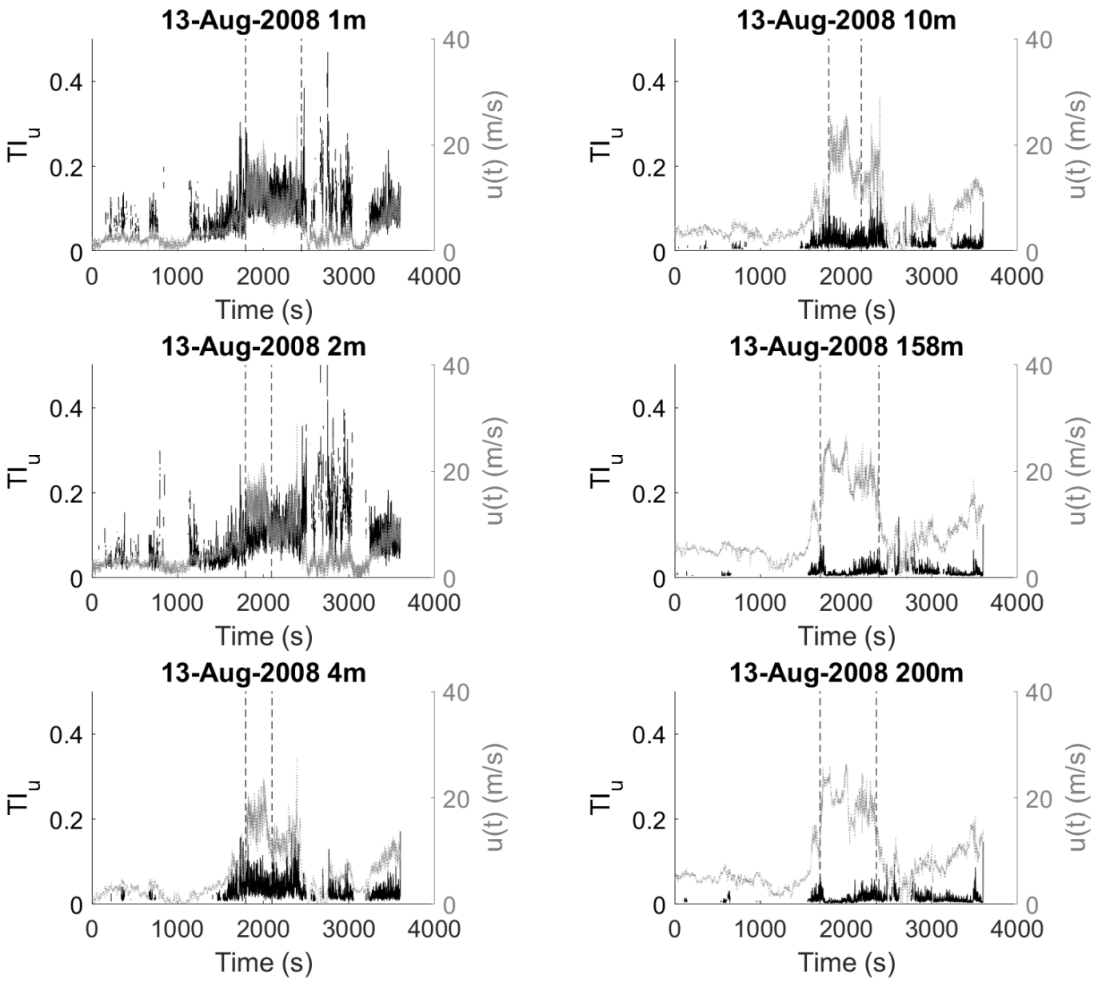

Figure 11 Wavelet turbulence intensity of the horizontal wind speed for the 13th August 2008 event at all measured heights (for clarity, turbulence intensity is only shown where $u(t) > U$, the overall mean horizontal wind speed). Vertical lines indicate the peak period.

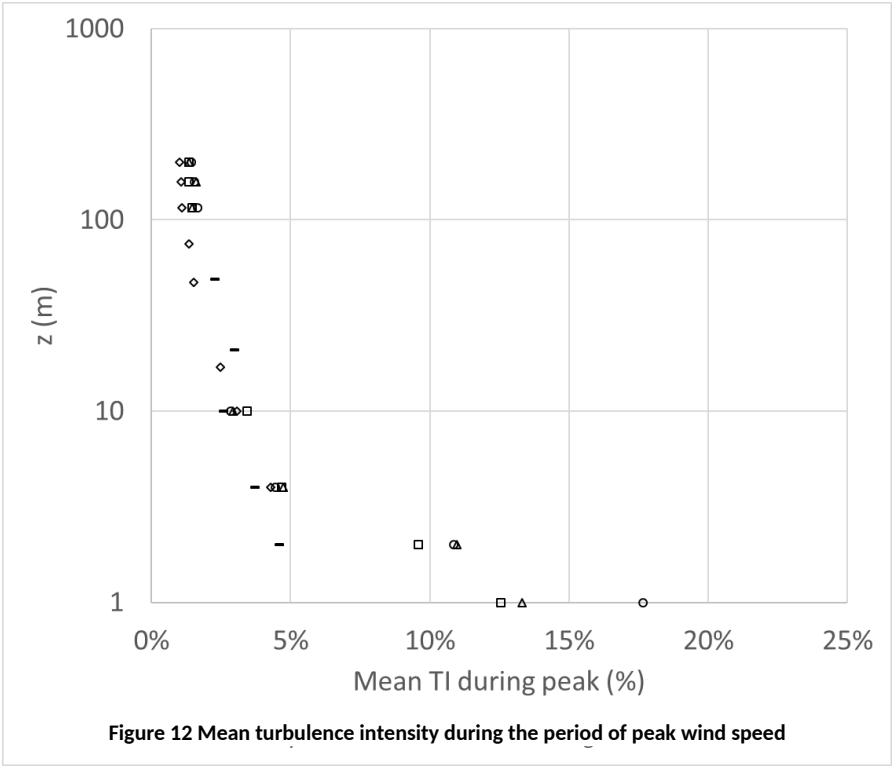

Figure 12 Mean turbulence intensity during the period of peak wind speed

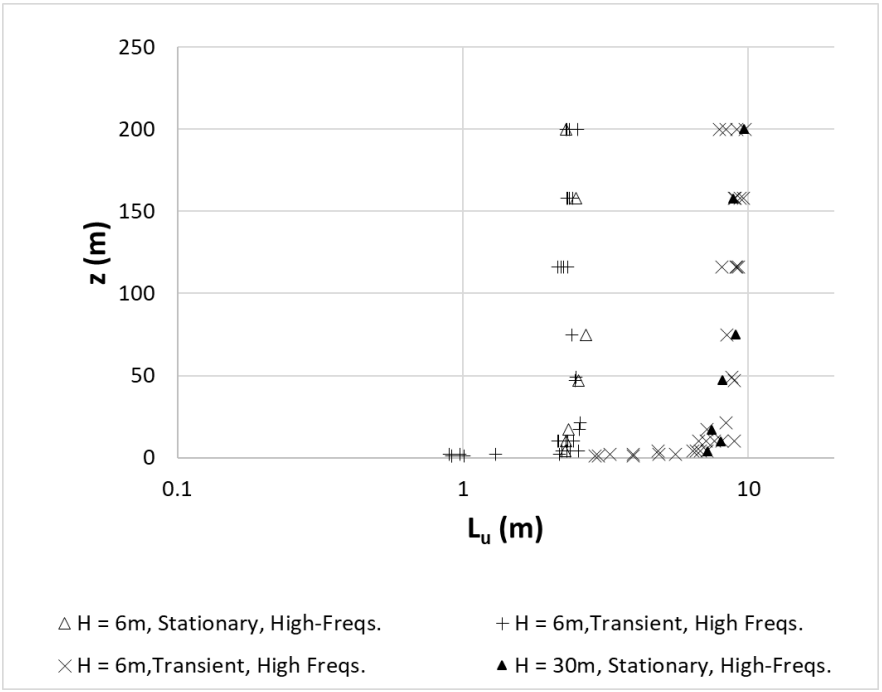

Figure 13 Integral length scales of turbulence for the high-frequency decomposition component

4.2.2 Vertical Component of Velocity

At low altitudes (< 10m; Figure 14) the magnitude of $w(t)$ increases during the peak period, reaching 10m/s. This mirrors the behaviour seen from event to event before the downburst, where $|w(t)|$ is approximately proportional to $u(t)$. As altitude increases, this period of increased vertical velocity extends to the deceleration phase of $u(t)$; maximum magnitude remains approximately unchanged (Figure 7), but the very small-scale turbulence (generated from ground roughness) has reduced. At the highest altitudes measured ($z > 116m$), $w(t)$ reaches 12m/s (21st May 2008 event) during the peak period and, in the case of the 13th August 2008 event, reaches 8m/s during the low horizontal speed region following the peak period (Figure 15).

Decomposition of the vertical wind speed illustrates this change with altitude from small-scale turbulence to larger scale effects. At low altitudes the low-frequency term is approximately zero, with some small (~1m/s) fluctuations appearing at $z = 10m$. At the high altitudes, low-frequency fluctuations dominate.

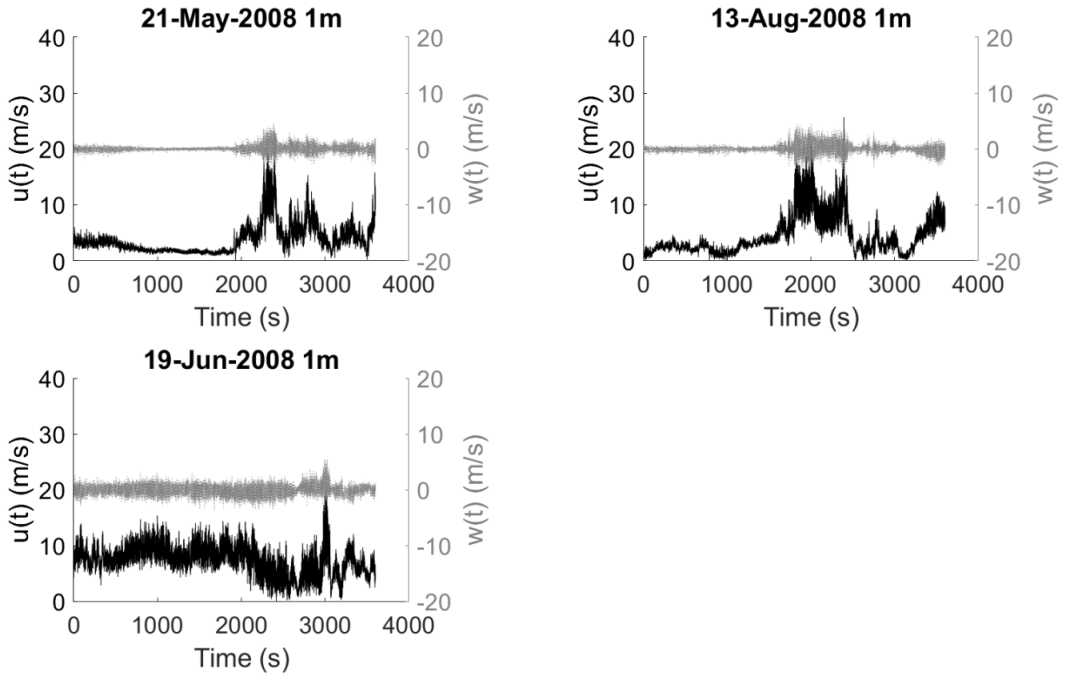

Figure 14 Wind speed time-histories at $\mathbf{z = 1m}$, all recorded events

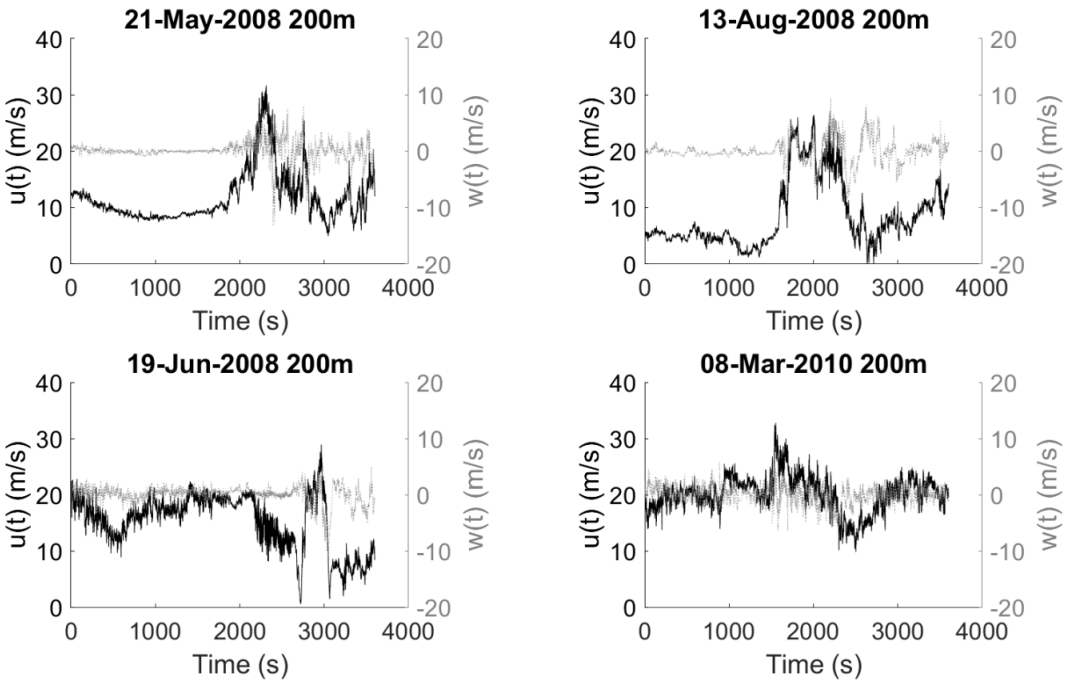

Figure 15 Wind speed histories at $\mathbf{z = 200m}$, all recorded events

To date, validation of physical simulations of downburst flow fields has compared only the horizontal wind speed to full-scale data, with the vertical component being neglected. The variation from event to event is large. During the 8th March 2010 event (Figure 16) the elevation angle was within $\pm 30°$ of horizontal at all heights. Generally, the range of angles is greater at low altitudes (Figure 17), though for the extreme elevation angles the magnitude is low ($< \sim 4m/s$), reduces at $z = 4m$ to $z = 10m$ (e.g. 13th August 2008 event, Figure 18) and then increases at high altitudes. Importantly, wind speeds $S(t) \cong 10m/s$ are seen for both upward ($\beta(t) \cong 280°$, 13th August 2008, $z = 158m$, Figure 18) and downward ($\beta(t) \cong 80°$, 19th June 2008, $z = 200m$, not shown) wind directions.

Figure 16 to Figure 18 were created from the low-frequency time-series and thus these extreme angle-speed combinations lie within those scales which are hypothesised to be modelable using the quasi-steady approach. Equivalent figures using the raw velocity data show similar elevation-wind speed characteristics, and neither give a clear insight into how long these high-speed, large-angle periods last; for this it is necessary to analyse the HSLE Duration data, defined in Section 3. Below 49m HSLE periods are only detected for the lowest thresholds ($S > S_{max}/4$, $\beta > 30°$ from horizontal), and for short durations (0.5 seconds or less). For 49m and higher (Figure 19) these periods of HSLE winds span the scales, with a minimum duration of 0.03s (equivalent to the sampling rate) but maximum durations in the tens of seconds at higher altitudes and thresholds of $S > S_{max}/3$ and $S > S_{max}/4$. If the speed threshold is set to $S > S_{max}/2$ or the elevation threshold is $45°$ then all HSLE periods are less than 3 seconds, the typical gust duration used for ABL flows. It is evident that low-rise and high-rise structures experience very different wind vectors during a downburst event. From this analysis it may be seen that low-rise and high-rise buildings experience very difference

600 wind fields during a downburst. The practical implications of these differences are discussed in the
601 following section.

602 It should be noted that the location of the anemometers relative to the downdraft impingement
603 point is unknown for the data presented in this paper, and almost certainly varies between events.
604 The fact that the above analysis is consistent across events indicates that, in terms of evaluating the
605 decomposition into low- and high-frequency components, this difference in relative position is
606 unimportant. Further, while there may be structural differences in the flow fields which cannot be
607 identified due to this limitation, in none of the cases examined do the data refute the assertion that
608 a quasi-steady/PTS approach is suitable. While some of the events (e.g. 8th March 2010) have
609 relatively low elevation angles, it is possible that (if measured at other relative positions) more
610 extreme angles would occur; the data from those events for which extreme elevation angles is
611 sufficient to show that further experiments to measure wind loading at such angles are necessary.

612

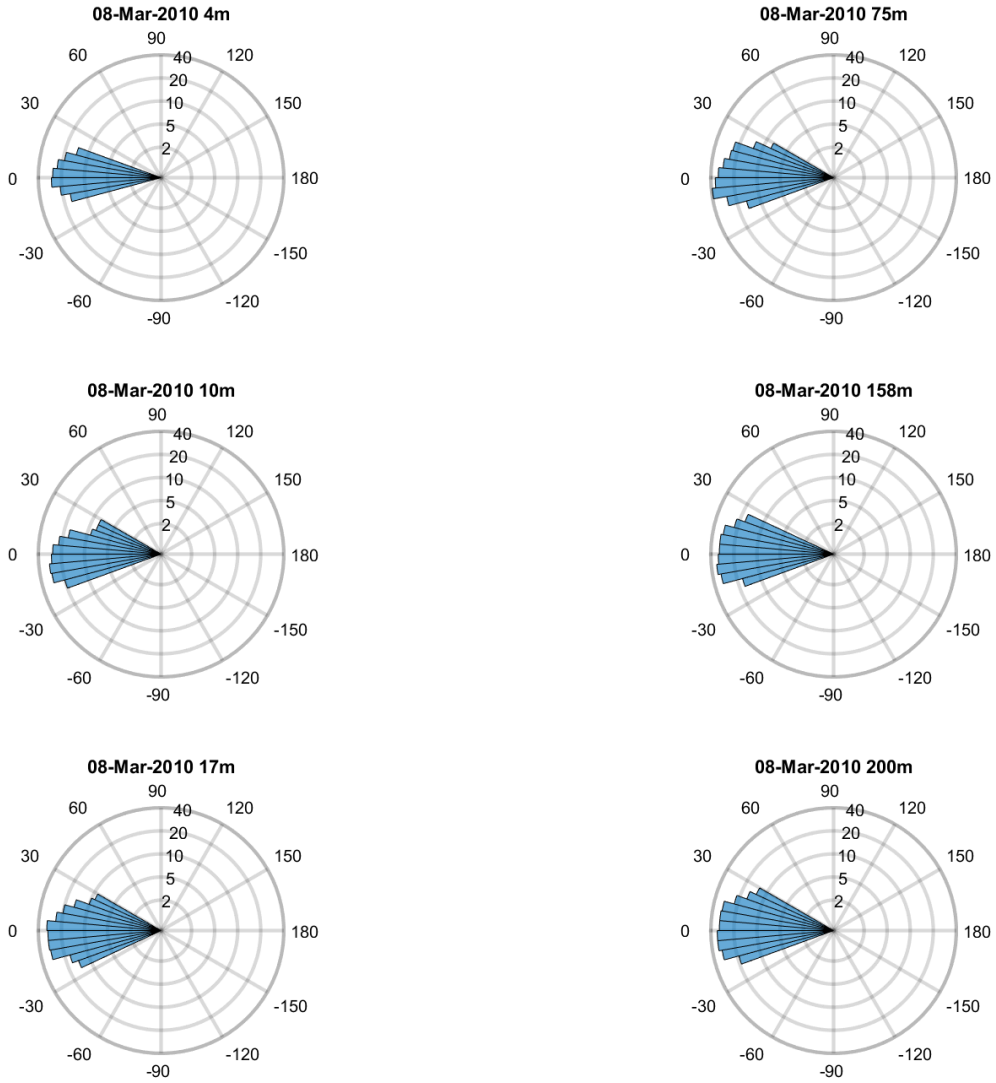

Figure 16 Maximum wind speed by elevation angle for the 8th March 2010 event (radial scale m/s and logarithmic)

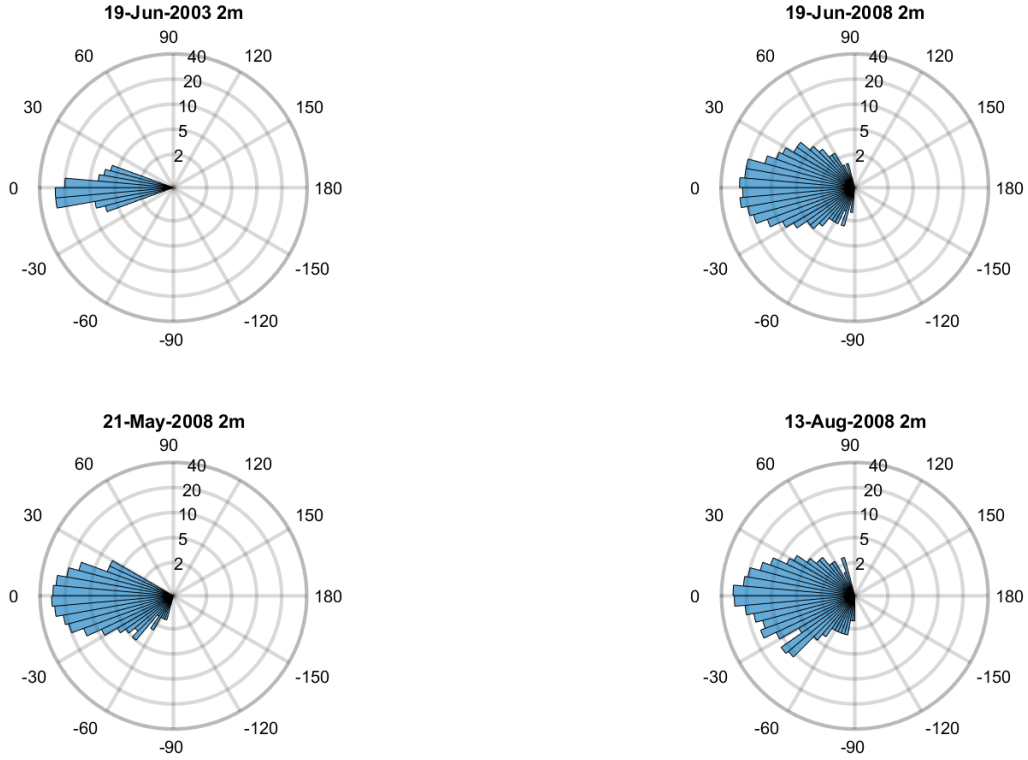

Figure 17 Maximum wind speed by elevation angle at $z = 2m$ (radial scale m/s and logarithmic)

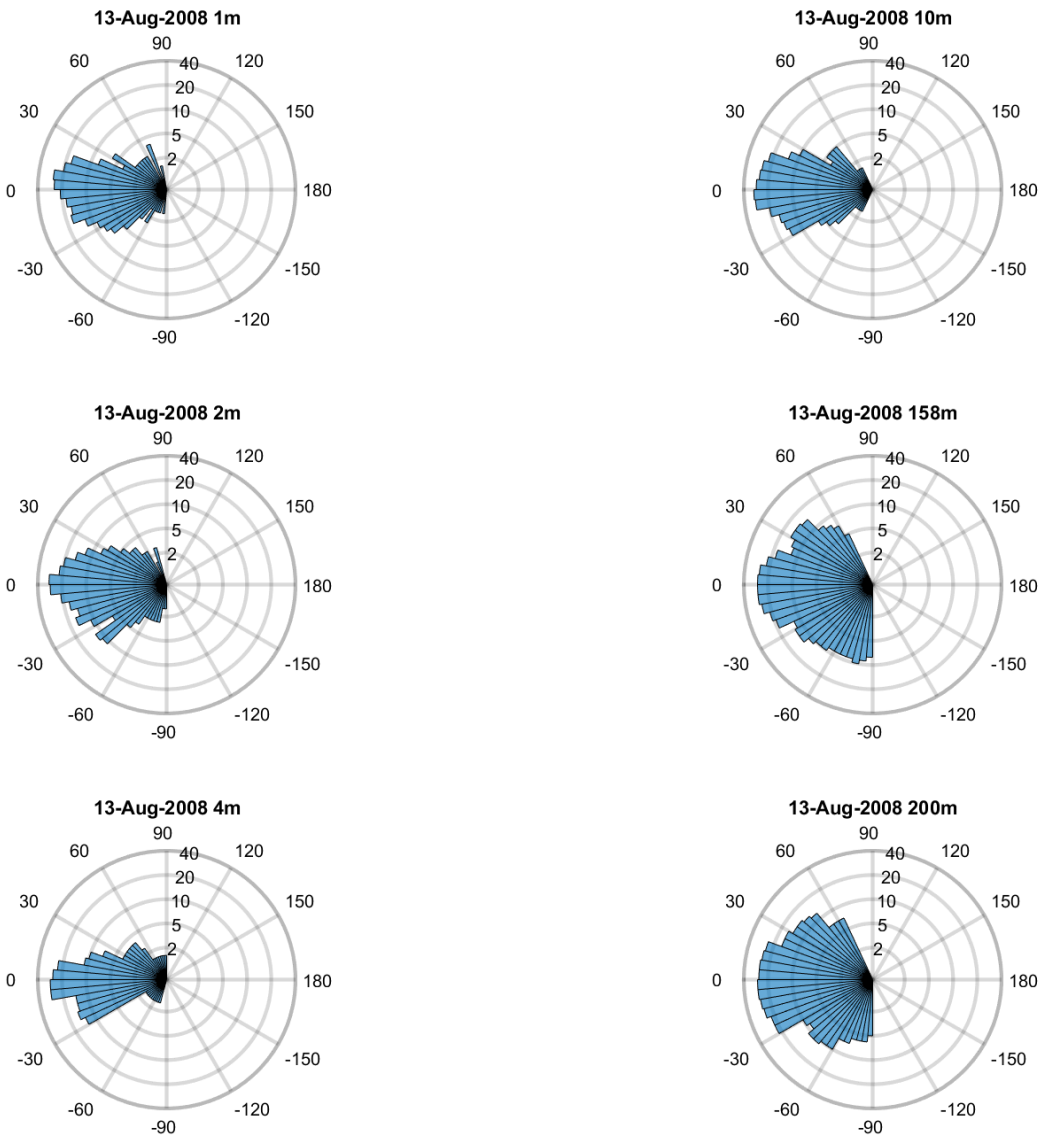

Figure 18 Maximum wind speed by elevation angle for the 13th August 2008 event (radial scale m/s and logarithmic)

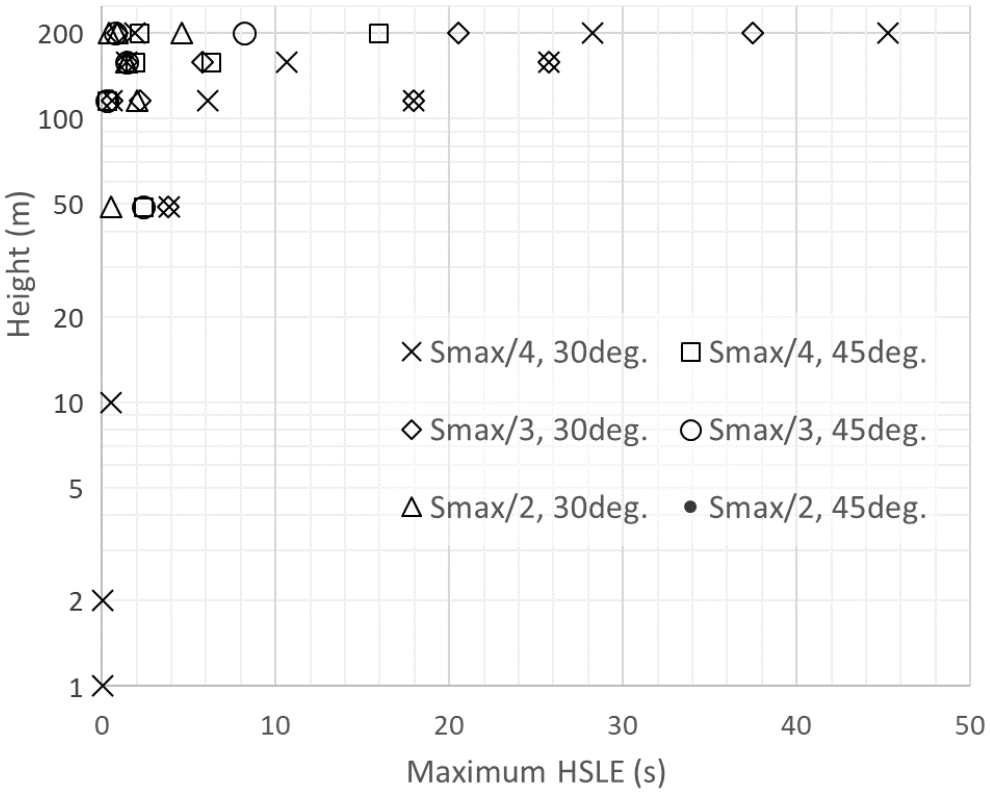

Figure 19 Maximum duration of high-speed, large-elevation events by height above ground

5 Application

For both low-rise and high-rise buildings, it is necessary to measure peak C_p values at a greater range of elevation angles and turbulence intensities, I_u, than is generally undertaken. This may be achieved using experimental methods similar to those detailed by Wu and Kopp (2018), and elevation angles spanning the range $-60° \leq \beta \leq 60°$ combined with $I_u(z_{fs} = 2m) \cong 10\%$ (subscript fs signifies full-scale equivalent) and $I_u(z_{fs} = 10m) \cong 3\%$ (see Figure 12). It should be emphasised that the I_u values presented in this paper are from the wavelet decomposition, and a similar process must be applied to evaluate this parameter for the wind tunnel. The process for obtaining the C_p values is outlined in Figure 20.

Due to the differences in the flow experienced by low-rise and high-rise buildings, each must be treated differently:

5.1 Low-Rise Buildings

The winds experienced by a low-rise building have durations similar to those of a typical ABL gust. In comparison to the scale of the large-scale vortex structures of a downburst ($\sim 1000m$), a low-rise building is small in height, and it is reasonable to assume that the flow direction is, in a mean sense, uniform over the building. Results from the tests outlined above may therefore be applied directly. The workflow is illustrated in Figure 21.

5.2 High-Rise Buildings

At heights above approximately $50m$, high-rise buildings may be subject to sustained, high speed winds at large elevation angles. It is suggested that the regions above and below $50m$ are treated separately for the evaluation of both local (component) loads and overall loading, with calculations reflecting the differences in wind speed, elevation angle and duration of the extremes of these.

In the measurement of the pressure coefficients, the use of building height, H, as the defining length is arguably inappropriate; for a building of height $200m$ the $5H$ cut-off scale is approximately the scale of the downdraft and ring vortex. The along-wind length may be a more appropriate representative length.

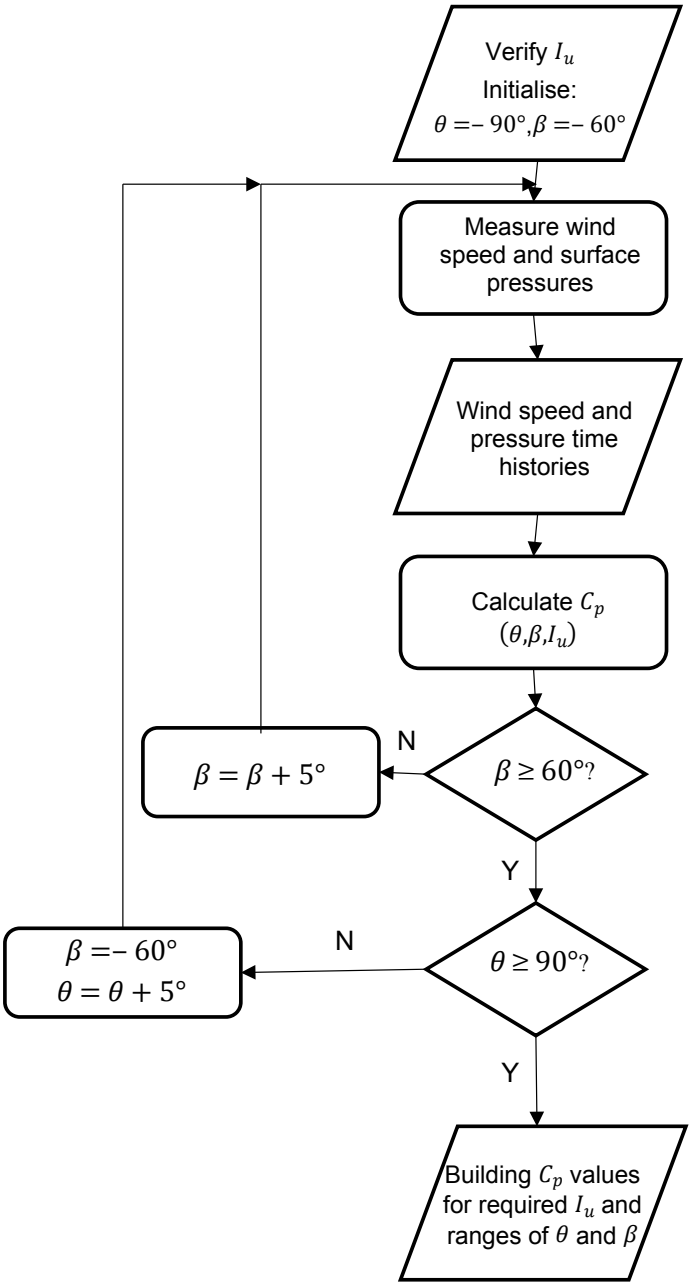

Figure 20 Process flow chart for measurement of peak $C_p$values

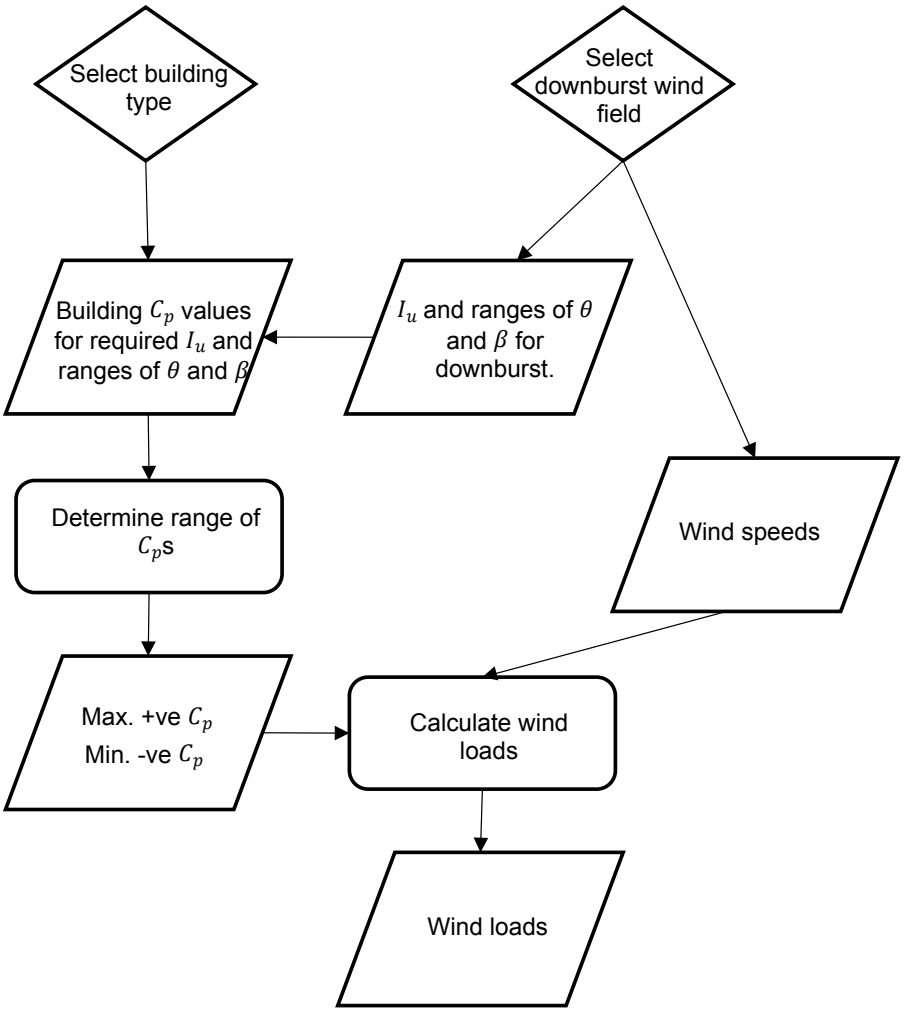

Figure 21 Wind loading calculation process flowchart

6 Conclusions

This novel research has examined the near surface wind field arising from full-scale thunderstorm downbursts. Aspects of Partial Turbulence Simulation have been applied to estimate a turbulence scale above which wind loading may be estimated by application of the quasi-steady theory, and below which wind tunnel tests are required to determine pressure coefficients. Horizontal and vertical velocity time-series were decomposed into high- and low-frequency components as defined by this scale. From this analysis it is concluded that:

1. Event-to-event variability of downbursts applies not only to the horizontal wind speed, but also to the large-scale variation of the vertical wind speed, and how this changes with respect to the peak horizontal field;
2. The main vortex structures of a downburst are large-scale by the above definition;
3. Although the magnitude of the high-frequency component varies with time, this variation is slow in relation to the frequencies making up the component, i.e. it is effectively a modulation of a stationary signal. The aerodynamic effects of the high-frequency components may, therefore, be estimated from steady wind tunnel simulations with appropriate turbulence;
4. Wind loading calculations for low-rise and high-rise buildings require different techniques, with the latter being somewhat more complex due to the variation of the flow field over the latter. In both cases, the suggested methodology for determining local pressure coefficients may be applied.

The above suggests that it is unnecessary to model the transient features of the wind field in physical simulations. This novel finding has considerable implications for the development of the subject, namely that bespoke, large-scale physical simulators are not required for such conditions.

Acknowledgements

The authors would like to thank the UK Engineering and Physical Science Research Council, which funded the University of Birmingham's original research on downbursts under grant number EP/J008281/1.

Appendix

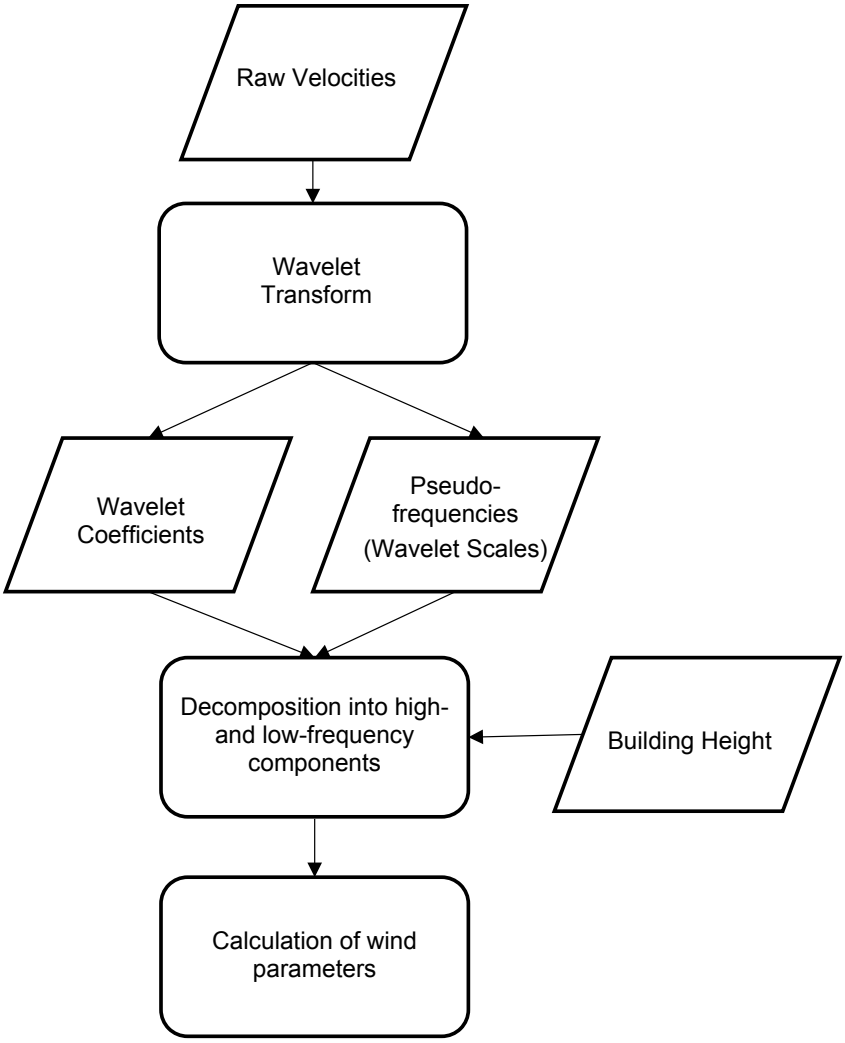

Figure 22 The wavelet decomposition process

References

Aboshosha, H., El Damatty, A., 2015. Engineering method for estimating the reactions of transmission line conductors under downburst winds. *Eng. Struct.* 99, 272–284. doi:10.1016/j.engstruct.2015.04.010

Asghari Mooneghi, M., Irwin, P., Gan Chowdhury, A., 2016. Partial turbulence simulation method for predicting peak wind loads on small structures and building appurtenances. *J. Wind Eng. Ind. Aerodyn.* 157, 47–62. doi:10.1016/j.jweia.2016.08.003

Butler, K., Cao, S., Tamura, Y., Kareem, A., Ozono, S., 2010. Characteristics of surface pressures on prisms immersed in a transient gust front flow field. *J. Wind Eng. Ind. Aerodyn.* 98, 299–316.

Butler, K., Kareem, A., 2007. Physical and numerical modeling of downburst generated gust fronts. *Proceedings of the 12th International Conference on Wind Engineering, Cairns, Australia*, pp. 791–798.

Chay, M.T., Letchford, C.W., 2002a. Pressure distributions on a cube in a simulated thunderstorm downburst - Part A: stationary downburst observations. *J. Wind Eng. Ind. Aerodyn.* 90, 711–732.

Chay, M.T., Letchford, C.W., 2002b. Pressure distributions on a cube in a simulated thunderstorm downburst - Part B: moving downburst observations. *J. Wind Eng. Ind. Aerodyn.* 90, 733–753.

Chen, L., Letchford, C.W., 2007. Numerical simulation of extreme winds from thunderstorm downbursts. *J. Wind Eng. Ind. Aerodyn.* 95, 977–990. doi:10.1016/j.jweia.2007.01.021

Chen, L., Letchford, C.W., 2005. Proper orthogonal decomposition of two vertical profiles of full-scale nonstationary downburst wind speeds. *J. Wind Eng. Ind. Aerodyn.* 93, 187–216. doi:10.1016/j.jweia.2004.11.004

Choi, E.C.C., 2004. Field measurement and experimental study of wind speed profile during thunderstorms. *J. Wind Eng. Ind. Aerodyn.* 92, 275–290. doi:10.1016/j.jweia.2003.12.001

Erickson, J., 2016. Continuous wavelet transform and inverse - File Exchange - MATLAB Central [WWW Document]. URL https://uk.mathworks.com/matlabcentral/fileexchange/20821 (accessed 8.8.18).

ESDU, 2001. IHS ESDU 85020: Atmospheric turbulence near ground: data for winds Amendment G [WWW Document]. URL https://www.esdu.com/cgi-bin/ps.pl?sess=birm_1181009111649xst&t=doc&p=esdu_85020g (accessed 10.9.18).

Fujita, T.T., 1985. Downburst: microburst and macroburst. *Univ. Chic. Press IL* pp.-p. 122.

Fujita, T.T., 1981. Tornadoes and downbursts in the context of generalized planetary scales. *J. Atmospheric Sci.* 38, 1511–1534.

Fujita, T.T., Wakimoto, R.M., 1981. Five scales of airflow associated with a series of downbursts on 16 July 1980. *Mon. Weather Rev.* 109, 1439–1456.

Gast, K.D., Schroeder, J.L., 2003. Supercell rear-flank downdraft as sampled in the 2002 thunderstorm outflow experiment. *11th International Conference on Wind Engineering*, ICWEIA, pp. 2233–2240.

Haines, M., Sterling, M., Quinn, A., 2013. Interference effects around two model high rise buildings in a simulated non-synoptic event. *European-African Conference on Wind Engineering*.

Hjelmfelt, M.R., 1988. Structure and life cycle of microburst outflows observed in Colorado. *J. Appl. Meteorol.* 27, 900–927.

Holmes, J.D., 2001. Wind Loading of Structures, Wind Loading of Structures. Spon Press.

Holmes, J.D., Hangan, H., Schroeder, J.L., Letchford, C.W., 2007. A forensic study of the Lubbock Reese downdraft of 2002. I. Storm characteristics. *12th International conference on Wind engineering and industrial aerodynamics*, Cairns, Australia.

Holmes, J.D., Hangan, H.M., Schroeder, J.L., Letchford, C.W., Orwig, K.D., 2008. A forensic study of the Lubbock-Reese downdraft of 2002. *Wind Struct.* 11, 137–152.

Jesson, M., Sterling, M., Letchford, C., Baker, C., 2015a. Aerodynamic forces on the roofs of low-, mid- and high-rise buildings subject to transient winds. *J. Wind Eng. Ind. Aerodyn.* 143, 42–49. doi:10.1016/j.jweia.2015.04.020

Jesson, M., Sterling, M., Letchford, C., Haines, M., 2015b. Aerodynamic forces on generic buildings subject to transient, downburst-type winds. *J. Wind Eng. Ind. Aerodyn.* 137, 58–68. doi:10.1016/j.jweia.2014.12.003

Kim, J., Hangan, H., 2007. Numerical simulations of impinging jets with application to downbursts. *J. Wind Eng. Ind. Aerodyn.* 95, 279–298. doi:10.1016/j.jweia.2006.07.002

Kwon, D., Kareem, A., 2009. Gust-front factor: new framework for wind load effects on structures. *J. Struct. Eng.* 135, 717–732. doi:10.1061/(asce)0733-9445(2009)135:6(717)

Letchford, C.W., Iverson, R.E., McDonald, J.R., 1993. The application of the Quasi-steady Theory to full scale measurements on the Texas Tech building. *J. Wind Eng. Ind. Aerodyn.* 48, 111–132. doi:10.1016/0167-6105(93)90284-U

Letchford, C.W., Marwood, R., 1997. On the influence of v and w component turbulence on roof pressures beneath conical vortices. *J. Wind Eng. Ind. Aerodyn.* 69–71, 567–577. doi:10.1016/S0167-6105(97)00187-6

Lin, W.E., Orf, L.G., Savory, E., Novacco, C., 2007. Proposed large-scale modelling of the transient features of a downburst outflow. *Wind Struct.* 10, 315–346.

Lombardo, F.T., 2009. *Analysis and Interpretation of Thunderstorm Wind Flow and its Effects on a Bluff Body* (PhD Thesis). Texas Tech University`.

Lombardo, F.T., Mason, M.S., de Alba, A.Z., 2018. Investigation of a downburst loading event on a full-scale low-rise building. *J. Wind Eng. Ind. Aerodyn.* 182, 272–285. doi:10.1016/j.jweia.2018.09.020

885 Lombardo, F.T., Smith, D.A., Schroeder, J.L., Mehta, K.C., 2014. Thunderstorm characteristics of
886 importance to wind engineering. *J. Wind Eng. Ind. Aerodyn.* 125, 121–132.
887 doi:10.1016/j.jweia.2013.12.004

888 Lundgren, T.S., Yao, J., Masour, N.N., 1992. Microburst modelling and scaling. *J. Fluid Mech.* 239,
889 461–488.

890 Mason, M.S., James, D.L., Letchford, C.W., 2009a. Wind pressure measurements on a cube subjected
891 to pulsed impinging jet flow. *Wind Struct.* 12, 77–88.

892 Mason, M.S., Wood, G.S., Fletcher, D.F., 2009b. Numerical simulation of downburst winds. *J. Wind*
893 *Eng. Ind. Aerodyn.* 97, 523–539.

894 McConville, A.C., Sterling, A.C., Baker, C.J., 2009. The physical simulation of thunderstorm
895 downdrafts using an impinging jet. *Wind Struct.* 12(2), 133–149.

896 Richards, P.J., Hoxey, R.P., 2004. Quasi-steady theory and point pressures on a cubic building. *J. Wind*
897 *Eng. Ind. Aerodyn.* 92, 1173–1190. doi:10.1016/j.jweia.2004.07.003

898 Richards, P.J., Hoxey, R.P., Short, L.J., 2001. Wind pressures on a 6m cube. *J. Wind Eng. Ind. Aerodyn.*
899 89, 1553–1564. doi:10.1016/S0167-6105(01)00139-8

900 Richards, P.J., Hoxey, R.P., Wanigaratne, B.S., 1995. The effect of directional variations on the
901 observed mean and rms pressure coefficients. *J. Wind Eng. Ind. Aerodyn.*, Third Asian-Pacific
902 Symposium on Wind Engineering 54–55, 359–367. doi:10.1016/0167-6105(94)00067-N

903 Shehata, A.Y., El Damatty, A.A., Savory, E., 2005. Finite element modeling of transmission line under
904 downburst wind loading. *Finite Elem. Anal. Des.* 42, 71–89. doi:10.1016/j.finel.2005.05.005

905 Solari, G., 2016. Thunderstorm response spectrum technique: theory and applications. *Eng. Struct.*
906 108, 28–46. doi:10.1016/j.engstruct.2015.11.012

907 Torrence, C., Compo, G.P., 1998. A practical guide to wavelet analysis. *Bull. Am. Meteorol. Soc.* 79,
908 61–78. doi:10.1175/1520-0477(1998)079<0061:apgtwa>2.0.co;2

909 Vermeire, B.C., Orf, L.G., Savory, E., 2011. Improved modelling of downburst outflows for wind
910 engineering applications using a cooling source approach. *J. Wind Eng. Ind. Aerodyn.* 99, 801–814.
911 doi:10.1016/j.jweia.2011.03.003

912 Wakimoto, R.M., Bringi, V.N., 1988. Dual-polarization observations of microbursts associated with
913 intense convection: the 20 July storm during the MIST project. *Mon. Weather Rev.* 116, 1521–1539.

914 Wang, L., 2007. *Stochastic modelling and simulation of transient events*. Notre Dame, Indiane, USA.

915 Wang, L., Kareem, A., 2004. Modeling of non-stationary winds in gust-fronts. *9th ASCE Specialty*
916 *Conference on Probabilistic Mechanics and Structural Reliability*, Albuquerque, New Mexico.

917 Wang, L., McCullough, M., Kareem, A., 2013. A data-driven approach for simulation of full-scale
918 downburst wind speeds. *J. Wind Eng. Ind. Aerodyn.* 123, Part A, 171–190.
919 doi:10.1016/j.jweia.2013.08.010

Wood, G.A., Kwok, K.C.S., Motteram, N.A., Fletcher, D.A., 2001. Physical and numerical modelling of thunderstorm downbursts. *J. Wind Eng. Ind. Aerodyn.* 89, 535–552.

Wu, C.-H., Kopp, G.A., 2018. A quasi-steady model to account for the effects of upstream turbulence characteristics on pressure fluctuations on a low-rise building. *J. Wind Eng. Ind. Aerodyn.* 179, 338–357. doi:10.1016/j.jweia.2018.06.014

Wu, C.-H., Kopp, G.A., 2016. Estimation of wind-induced pressures on a low-rise building using quasi-steady theory. *Front. Built Environ.* 2. doi:10.3389/fbuil.2016.00005

Zhang, S., Solari, G., De Gaetano, P., Burlando, M., Repetto, M.P., 2018. A refined analysis of thunderstorm outflow characteristics relevant to the wind loading of structures. *Probabilistic Eng. Mech.*, ISM 2016 54, 9–24. doi:10.1016/j.probengmech.2017.06.003

Zhang, Y., Hu, H., Sarkar, P.P., 2014. Comparison of microburst-wind loads on low-rise structures of various geometric shapes. *J. Wind Eng. Ind. Aerodyn.* 133, 181–190. doi:10.1016/j.jweia.2014.06.012

Zhang, Y., Sarkar, P., Hu, H., 2013. An experimental study of flow fields and wind loads on gable-roof building models in microburst-like wind. *Exp. Fluids* 54, 1–21. doi:10.1007/s00348-013-1511-9